

Contents lists available at ScienceDirect

Acta Materialia

journal homepage: www.elsevier.com/locate/actamat



Full length article

The effect of chemical disorder on defect formation and migration in disordered max phases



Prashant Singh*, Daniel Sauceda, Raymundo Arroyave

Department of Materials Science & Engineering, Texas A&M University, College Station, TX 77843, USA

ARTICLE INFO

Article history:
Received 6 August 2019
Revised 18 October 2019
Accepted 13 November 2019
Available online 15 November 2019

Keywords:
Disorder
Max phase
Point-defects
Vacancy-diffusion
Density-functional theory

ABSTRACT

MAX phases have attracted increased attention due to their unique combination of ceramic and metallic properties. Point-defects are known to play a vital role in the structural, electronic and transport properties of alloys in general and this system in particular. As some MAX phases have been shown to be stable in non-stoichiometric compositions, it is likely that such alloying effects will affect the behavior of lattice point defects. This problem, however, remains relatively unexplored. In this work, we investigate the alloying effects on the structural-stability, energy-stability, electronic-structure, and diffusion barrier for point defects in MAX phases within a first-principles density functional theory framework. The vacancy (V_M, V_A, V_X) and antisite (M-A; M-X) defects are considered with M and A site disorder in $(Zr-M)_2(AA')C$, where M=Cr,Nb,Ti and AA'=Al, Al-Sn, Pb-Bi. Our calculations suggest that the chemical disorder helps lower the V_A formation energies compared to V_M and V_X . The V_A diffusion barrier is also significantly reduced for M-site disorder compared to their ordered counterpart. This is a very important finding because the reduced barrier height will ease the Al diffusion at high-operating temperatures, which will help the formation of passivating oxide layer (i.e., Al_2O_3 in aluminum-based MAX phases) and will slow down or stop the material degradation. We believe that our study provides a fundamental understanding and an approach to tailor the key properties that can lead to the discovery of new MAX phases.

© 2019 Acta Materialia Inc. Published by Elsevier Ltd. All rights reserved.

1. Introduction

Research in high-temperature structural materials is gaining momentum due to the ongoing quest for ever increasing operating efficiencies in power generation technologies [1]. An example is the nuclear power industry, which seeks new reactor designs that in turn demand structural and coating materials capable of withstanding higher operating temperatures at higher irradiation conditions. MAX phases are a new class of high-temperature materials with the general formula $M_{n+1}AX_n$ [n = 1,3; M=transition element; A = A-group, and X = C or N]. Their high-temperature thermodynamic and structural stability, damage-tolerance and oxidation-resistance [2-5] make MAX-phases a potential candidate structural material for nuclear applications [6]. Beyond structural and coating applications, research on MAX phases has also led to the discovery of MXenes based on the selective leaching of the A element [7,8]. Many MAX phase (and MXene) properties of interest in these materials depend on the nature and behavior of point defects within the lattice.

In the past, irradiation has been shown to significantly alter the microstructures of systems through the creation of point defects [9-12]. For example, in the context of nuclear applications, irradiation degrades the material by damage accumulation. These defects interact with other defects and atoms within the solid-solution while they migrate through the lattice [13]. It is thus to be expected that understanding the behavior (extrinsic or intrinsic) of point defects in MAX phases is important if one is to understand the factors controlling their performance under irradiation environments. In many materials systems, chemical-disorder induced alloy complexity is another factor that can significantly impact the defect evolution, energy dissipation, and radiation resistance [14–17] that arises from the interaction of (energetic) ions with solids in a radiation environment.

Following the trends observed in the development of other materials systems, recent efforts on the synthesis, characterization and modeling of MAX phases have focused on the expansion of their composition palette through mixing in the different sublattices of the MAX phase crystal system. While some work has already been carried out in understanding the energetics and behavior of point defects in stoichiometric MAX phases [12], the investigation of defect physics of disordered MAX phases remains

^{*} Corresponding author. E-mail address: psingh84@tamu.edu (P. Singh).

relatively unexplored relative to other materials systems. Therefore, it becomes desirable to investigate the interplay of disorder and the point defects in order to develop an understanding towards the microstructural changes due to irradiation for the future nuclear structural materials [18–27]. Recent studies show that disorder can be used to manipulate alloying behavior to achieve desirable physical and chemical properties, e.g., thermoelectriceffects [28], charge-transport [29], and magnetoresistance [30]. The tailoring of properties in these applications ultimately arises from the strong connection between chemical disorder and the stability of point defects. It is thus to be expected that, in a similar fashion, chemical disorder in MAX phases can play an important role in determining the local configuration, formation energetics and migration behavior of point defects.

In this work, we discuss the impact of chemical disorder on the stability and diffusion of point defects in MAX phases. Five MAX phase solid solution systems [based on the stoichiometry M2AlC, M=Ti, Zr, Nb, Cr, Ta (for Ta see supplement)] of the 211 chemistry are chosen to investigate the connection between alloying and point defect behavior. We investigate the effect of single-site (M-, or A-), and two-site (M- & A-) disorder on the energetics and migration behavior of point defects. Our calculations show, for example, that modifying chemical disorder leads to notable changes on the defect formation and migration energies. Our focus remains on Al-containing MAX phases due to their superior oxidation resistance, which results from the formation (in some of these compounds) of stable alumina-based passivating layers that protect them from further oxidation [31]. We used the first-principles density functional theory and climbing nudge elastic band (cNEB) schemes to study V_M, V_A and V_C vacancy-mediated diffusion in $(Zr-M)_2AIC$ and $(Zr-M)_2(AA')C$, where M=Cr,Nb,Ti and A-A'=AI, AI-D'Sn, Pb-Bi. Zr-containing MAX phases were selected because they have already been identified as candidate materials for nuclear structural applications. A detailed discussion about the dependence of the migration energy on the alloying elements and defects is provided. We also investigate the responsible electronic structure features that control the properties of defects and its connection to elemental properties, such as, atomic-radii and electronegativity.

2. Computational details

While in the context of Density Functional Theory (DFT) there are many ways to account for the chemical disorder in a crystal structure, however, the use of periodic supercells to mimic disordered configurations constitute the most common method to compute the electronic and structural properties of disorder materials with and without defects [32]. Here, we make use of the special quasi-random supercell structures (SQS) to model disordered MAX phase supercells as implemented within the Alloy Theoretic Automated Toolkit (ATAT) [33]. SQS are periodic unit cells in which atomic occupancy is engineered to match as close as possible the statistics of truly random alloys at the same chemical composition. The quality of the generated SQS (periodically repeated) supercell is quantified by the correlation function (we choose two and three body interactions to achieve best correlation function).

In this work, an SQS of 200 atoms has been generated to mimic disorder on M-, A- and/or X-sublattices of MAX phases. Both cationic and anionic vacancy defects are considered in the disordered configurations (M-M')₂(A-A')(X-X'). Antisite pairs are created by interchanging the M (A) or A (M) atoms within neighboring layers. We note here that while smaller cells could have been used, the selected supercell size of O(10²) is necessary in order to accurately compute the energetics of periodic structures without the pathologies arising from their periodic images [34,35].

We use first-principles density functional theory as implemented in Vienna *Ab-initio* Simulation Package (VASP) [36,37] to

study structural properties, electronic properties and vacancy diffusion in disorder MAX phases. The gamma-centered Monkhorst-Pack [38] k-mesh of $1 \times 1 \times 1$ and $3 \times 3 \times 3$ is used for Brillouin zone integration during geometry-optimization and charge self-consistency, respectively. Total energies and forces are converged to 10^{-5} eV/cell and -0.001 eV/A, respectively. The Perdew, Burke and Ernzerhof (PBE) generalized gradient approximation is used with a planewave cut-off energy of 533 eV [39].

The vacancy formation energy (E_{form}^{Vac}) in MAX phases is defined as:

$$E_{form}^{Vac}(V_{M/A/X}) = E_{tot}(V_{M/A/X}) - E_{tot}(MAX) + \mu_{M/A/X}$$

where M/A/X, M (=Ti, Ta, Cr, Nb, Zr), A=Al, X = C. E tot (V_{M/A/X}) is the calculated total energy of a cell with defect and $E_{tot}(\mbox{MAX})$ is the total energy of a pure MAX phase without defects, and $\mu_{M/A/X}$ is the chemical potential of $V_{M/A/X}.$ For the calculation of defect energies, we use the chemical potential of an isolated gas-phase atom and consider the vacancy defects as charge-neutral due to metallic nature of MAX phases. The chemical potential of isolated atoms is calculated in the same MAX phase SQS supercell by keeping M/A/X atoms at the center of the unit-cell. For this work, we decided not to include the entropic effects arising from thermally excited degrees of freedom because the energy scales (for the formation of defects and migration energies) tend to be in the order of 100 meV and above, with some processes requiring energies well above 4 eV. Therefore, the major conclusions are unlikely to change wheather or not one explicitly accounts for the entropic corrections.

The defect migration (or diffusion barrier) energies are calculated using the cNEB method [40] as implemented in VASP. The cNEB method can be used to identify the minimum energy path of migrating defects from one site to another site within the same unit cell by essentially identifying the set of configurations along the path with vanishingly small atomic forces normal to the path itself. Thus, the cNEB method allows us to understand plausible mechanisms for defect migration as well as the energy barriers associated to these atomic long-range displacements. This information is important not only to understand the kinetics of defect evolution but can also contribute to better understanding and identification of plausible atomic mechanisms leading to defect recovery [41]. Here, the vacancy migration energies in ordered and disordered MAX phase crystals is determined by a transition state search, where the initial and final states are relaxed structures with one vacancy, respectively. We use 6 intermediate images to accurately calculate the migration energy barrier of MAX phases [42] from the lowest energy position to the other symmetry equivalent position.

3. Results and discussion

3.1. Structural properties and formation energies of ordered max phases with and without vacancies

M₂AlC phase forms a hexagonal structure (space-group=P6₃/mmc) that consists of edge-sharing M₆X (*M*=cation, *X*=anion) octahedra interleaved with cation (A)-layer. The octahedra are isostructrual to the rock salt binary carbides. While our interest is on disordered MAX phases, we first present structural and energy stability of ordered MAX phases and respective vacancy cases. Table I shows the ground-state structural properties and effect of vacancy on M₂AlC, where *M*=Cr,Ta,Nb,Ti,Zr. We compute the equilibrium lattice configurations of each case and find good agreement with experimentally known MAX phases [43-46], ensuring the reliability and accuracy of our calculations. We allow the vacancy supercell to relax homogeneously to the ground state

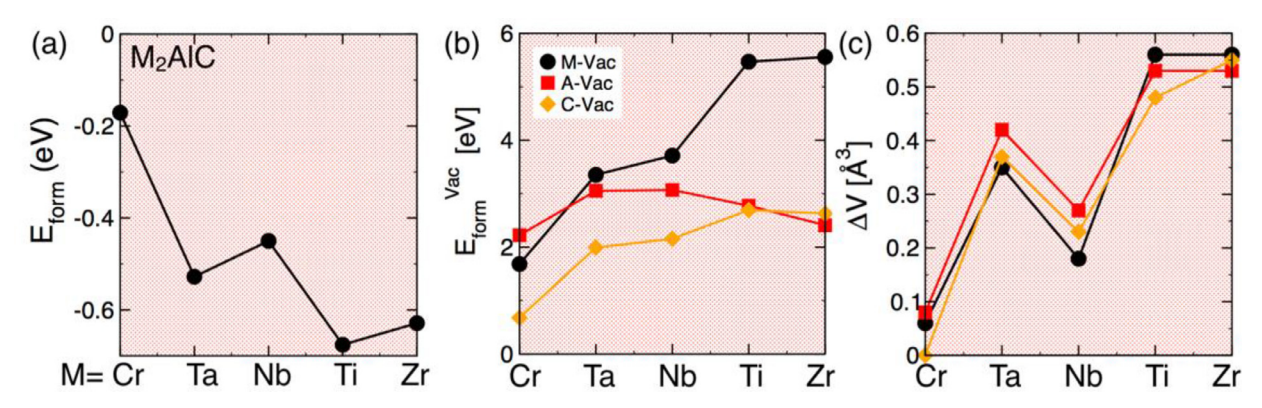


Fig. 1. The formation enthalpy of (a) pure and (b) vacancy (V_M, V_A, V_X) M_2 AlC MAX phases, M = Cr, Ta, Nb, Ti, Zr. (c) Volume change of vacancy MAX phase with respect novacancy cases.

energies before evaluating the complete set of the elastic constants. In Table. S1, we list the elastic constants (C_{ij}), bulk modulus (K), shear modulus (G), Young's modulus I, Poisson ratio (ν) and Pugh ratio k=G/K as obtained by Voigt-Reuss-Hill approximation [47]. The lower Pugh (k) ratio for some MAX phases indicates relative brittleness compared to other chemistries. Comparing the bulk moduli of Zr_2AlC with Nb_2AlC from Table S1 shows that Nb_2AlC is elastically much stiffer than usually known allotropes. This is because Nb_2AlC has larger elastic moduli all across: a bulk modulus of 170 GPa, a shear modulus of 119 GPa and a Young's modulus of 290 GPa compared to Zr_2AlC .

In Fig. 1, we show (a) the formation enthalpy of ordered MAX phases, (b) defect stability (E_{form}^{Vac}), and (c) relative change in cell volume [$\Delta V=V_{final}(M_2AlC\text{-vacancy})$ - $V_{initial}(M_2AlC)$] between pure and defect-containing structures. The formation energy (E_{form}) in Fig. 1a suggests that Ti- and Zr-based MAX alloys are more stable-relative to their elemental constituents-than their other transition metal counterparts. The large V_{M} and V_{C} vacancy formation energies in Fig. 1b makes it harder to create M-& C-vacancies for Ti₂AlC and Zr₂AlC. On other hand, the A-site vacancy formation is less energetically favorable in Nb2AlC and Ta2AlC. The volume of the MAX phase, in Fig. 1c, is sensitive to the vacancy with positive ΔV . The Cr_2AlC with V_C is the only exception in Fig. 1c that shows either very small or no change in volume (attributed to magnetic character of Cr). If we make a comparison, the stable phases in Fig. 1b have smaller shear and Young's moduli (see Table. S1). The Poisson's ratio of most of the ordered and vacancy MAX phases lie within the usual MAX phase range, i.e., from 0.200 to 0.260. The Pugh ratio (k) for crystalline Ti₂AlC (1.29) is smaller than other MAX phases, while some vacancy-containing alloys in Table S1 are fairly large. This indicates that those phases are relatively close to the ductile regime-here we note that the ability of MAX phases to undergo significant deformation is the result of complex mechanisms that require analysis well beyond the relatively simplistic metrics of bulk and shear modulus and that remain outside the scope of this work.

A major focus of our work is to look at the effect of chemical alloying on the formation energy, vacancy stability and vacancy migration of disordered MAX phases. As mentioned above, the fact that MAX phases can be synthesized with solid solutions on the M, A, or X sites greatly increases their chemical versatility and significantly expands the MAX phase composition space. In order to emulate disordered solid solutions, we designed an SQS supercell with 50:50 disorder with no vacancy on M-site, and M-&A-site to test the $E_{\rm form}$ with their ordered counterparts. The calculated $E_{\rm form}$ of $(Zr-M)_2AlC$ and $(Zr-M)_2(A-A')C$ are shown in Fig. 2 where M=Cr, Nb, Ti and A-A' =Sn-Al, Pb-Bi. The horizonal lines in Fig. 2 represents $E_{\rm form}$ of the ordered phase. For example, alloying M-site

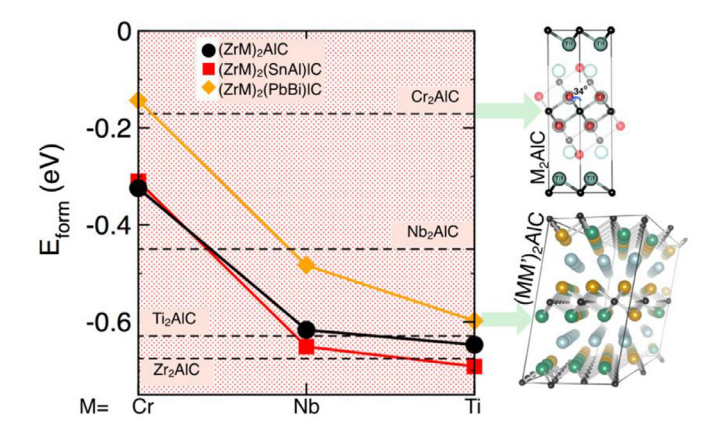


Fig. 2. Formation enthalpy (E_{form}) of MAX phase for M-site disorder and horizonal dashed (black) lines represent order MAX-phase E_{form} . Right-panel shows (top) ordered, M_2AlC , and (bottom) disordered (M-M')₂AlC supercell. Note that comparison with formation energies of pure MAX phases is just qualitative as we have not computed the convex hull against all possible phases in these systems.

in Nb₂AlC with Zr stabilizes the $(ZrNb)_2AlC$ by -0.2 eV/atom, however, if we think of alloying the M-site in Zr₂AlC with Nb this slightly reduces the stability by + 0.05 eV/atom. This indicates the tendency of C-Nb-Al to order while C-Zr-Al tends to cluster compared to their ordered counterpart. The overall picture of negative formation energy shows the thermodynamic stability of each of disordered MAX phase, relative to their elemental constituents, considered in this study. Our simulations also suggest that the compositional dependence of the energy of mixing is complex and non-ideal [48]. The minimum in the energy of mixing obtained for ordered (Fig. 1) and disordered (Fig. 2) MAX phases is consistent with the existence of a solubility limit.

3.2. Vacancy defects

In this section, we discuss the effect of vacancies on volume and E_{form}^{Vac} of pure and disordered MAX phases. We investigated three types of vacancies, i.e., $V_{\rm M}$, $V_{\rm A}$ and $V_{\rm X}$. Fig. 3 (a,c,e) shows the trends of positive volume change with respect to no-vacancy disorder MAX phases. Point-defects can lead to overall change in volume with respect to ideal cell, e.g., the defects in nuclear graphite induced by irradiation increases the $c_{\rm lat}$ and decreases ($a_{\rm lat}$ & $b_{\rm lat}$) in [0001] plane in response to interstitial carbons. The introduction of vacancies increases the volume as shown in Figs. 1c & 3. However, our calculations found that the Cr or Nb based MAX phases are the only exceptions that shows a drop in relative volume with respect to

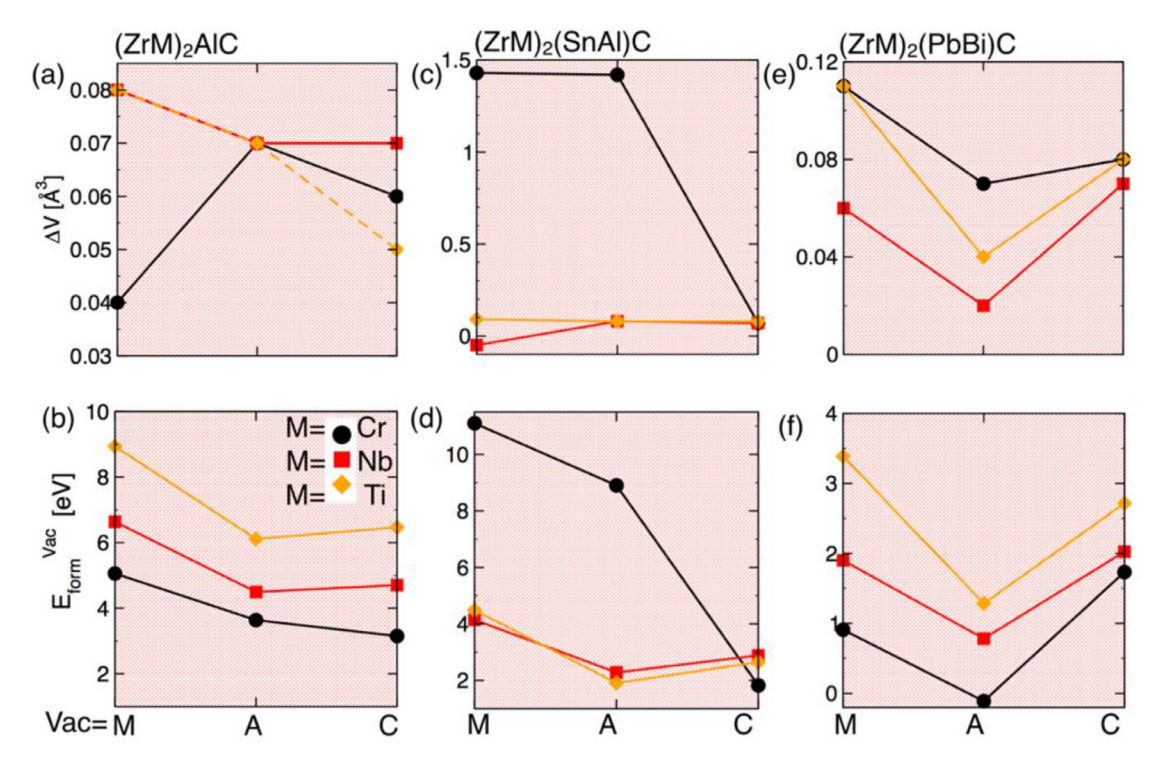


Fig. 3. The effect of vacancy on volume and vacancy formation energy of disorder MAX phase. We consider M-and A-site disorder along with three possible vacancy scenarios: V_M , V_A and V_X . We consider $(Zr-M)_2AIC$ and $(Zr-M)_2(A-A')C$ cases where M=Cr, Nb, & Ti, and A-A'=Sn-AI & Pb-Bi, respectively.

other cases. For two-site disorder, $(ZrNb)_2(SnAl)C$ shows negative change in total volume compared to parent phase. Although, the change in volume is very small but a significant drop in E_{form}^{Vac} is found compared to single-site disorder. The calculated E_{form}^{Vac} in Fig. 3(b,d,f) shows that V_M in $(ZrTi)_2AlC$ are difficult to form compared to $(ZrNb)_2AlC$ and $(ZrCr)_2AlC$, i.e., E_{form}^{Vac} [$(ZrTi)_2AlC$] > E_{form}^{Vac} [$(ZrNb)_2AlC$] > E_{form}^{Vac} [$(ZrCr)_2AlC$]. However, the E_{form}^{Vac} is lower for two-site disorder in $(ZrM)_2[AA']C$, where M=Cr,Nb,Ti and AA'=Sn-Al, Pb-Bi, i.e., vacancy creation is easier compared to the single-site disorder. The $(ZrCr)_2(SnAl)C$ is the only exception, where two-site disorder increases V_M and V_A E_{form}^{Vac} compared to $(ZrNb)_2(SnAl)C$] and $(ZrTi)_2(SnAl)C$] have competing E_{form}^{Vac} as shown Fig. 3d. The E_{form}^{Vac} trend in Fig. 3f for $[(ZrM)_2(PbBi)C]$ is significantly reduced compared to Fig. 3b: E_{form}^{Vac} [$(ZrTi)_2(PbBi)C$] > E_{form}^{Vac} [$(ZrNb)_2(PbBi)C$] or E_{form}^{Vac} [$(ZrCr)_2(PbBi)C$], i.e., it is easier to create V_A vacancies compared V_X in $(ZrCr)_2AlC$.

For M=Cr, Nb and Ti in $(Zr-M)_2AlC$, the E_{form}^{Vac} approximately follows the trend $[E(V_M) > E(V_A) > E(V_X)]$, $[E(V_M) > E(V_X) > E(V_X)]$ $E(V_A)$] and $E(V_M) > E(V_X) > E(V_A)$ for M=Ti, respectively. Notably, E_{form}^{Vac} depends strongly on choice of atomic $\mu_{M/A/X}$. This is the reason, E_{form}^{Vac} for V_A , and/or V_C is lower in $(Zr-M)_2AlC$ than $(Zr-M)_2AlC$ $M_2(SnAl)C$ or $[(Zr-M)_2(PbBi)C$ as shown Fig. 3d & f. The V_{Zr} is the least affected while V_C is the most affected defect in disordered MAX phases due to the respective atomic $\mu_{Zr/C}$. Therefore, irrespective of the choice of μ in ordered MAX phase, it is difficult to create V_{Zr} as shown in Fig. 1b. Depending on choice of disorder, V_{Zr} becomes relatively easier to form, while it is harder to create V_A compared to V_X in Zr_2AlC . Consequently, the synthesis condition, i.e., choice of μ , decides the relative stability of V_{Al} or V_{C} in $\text{Zr}_{2}\text{AlC}.$ Contrastingly, choice of μ on other MAX phases has a negligible effect on the E_{form}^{Vac} , where V_C remain the most stable defect configurations.

3.3. Antisite defects

The $E_{form}^{antisite}$ indicates the difficulty of antisite defect formation and irradiation incited recovery mechanism, which depends on the vacancy types and the target sublattices. The effect of antisite defects on volume (ΔV), energy stability and charge density difference of pure and defected MAX phases are shown in Fig. 4a & 4b for $(Zr-M)_2AIC$. The $E_{form}^{antisite}$ do not have significant dependence on the atomic configuration as the atomic species are only interchanged, i.e., no atoms are moved in-or-out of the chemical reservoir. We show in Fig. 4a that M-Al antisite pair does not affect ΔV , but the exchange between M and X increases the volume – with Ti-C as the only exception that shows negative ΔV . Antisite defects leads to positive ΔV for $(ZrCr)_2AlC$ while negative ΔV for $(ZrCr)_2AlC$ and $(ZrTi)_2AlC$. Based on $E_{form}^{Antisite}$ in Fig. 4b, the antisite pairs at M=Zr (Zr-C or Zr-Al) are more difficult to form compared to M=Cr. Comparison of $E_{form}^{Antisite}$ (Fig. 4b) with E_{form}^{Vac} (Fig. 3b) suggests that M=Cr based antisite pairs are energetically more favorable due to lower energy cost.

We can understand this in terms of empirical parameters, such as, electronegativity (χ) and atomi-radii (R). Here, the electronegativity difference $(\Delta \chi)$ of two atoms can tell us about the displacement of charges when two chemical species are mixed together. For example, in (ZrCr)_2AlC, $\Delta\chi_{\text{Cr-Al}}$ is less than $\Delta\chi_{\text{Zr-Al}}$ or $\Delta\chi_{Zr\text{-Al}}$ for $\chi_{Zr}=$ 1.33, $\chi_{Cr}=$ 1.66, $\chi_{Al}=$ 1.61, and $\chi_{C}=$ 2.5 and atomic-radii difference (ΔR) of Cr-Al is less than Zr-C or Al-C for $R_{Zr} =$ 0.86 Å, $R_{Cr} =$ 0.76 Å, $R_{Al} =$ 0.53 Å, and $R_{C} =$ 0.29 Å, respectively. The large difference in ΔR (62% vs 43%) and $\Delta \chi$ (21% vs 3%)) while comparing Zr-Al with Cr-Al explains the higher energy cost to create Zr-Al antisite pairs in (ZrCr)2AlC. However, smaller $\Delta \chi$ and ΔR for Cr-Al suggest that Cr-Al antisite pairs are preferred over Zr-Al, where electronic effects play a pivotal role. Clearly, the C-layer is not energetically favorable for Zr/Cr or Al for antisite defect formation, therefore, it creates a vacancy by migrating into the next available cation M- (or A) layer. This shows

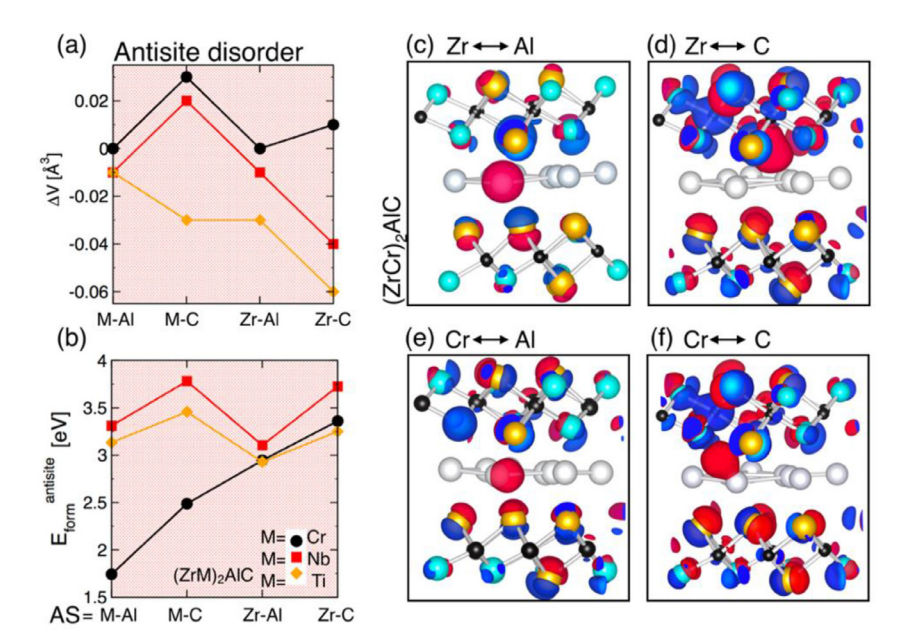


Fig. 4. Effect of antisite defects on (a) cell volume and (b) formation energies of $(ZrM)_2AIC$, where M=Cr,Nb,TI. (c-f) Charge density difference between $(ZrM)_2AIC$ antisite defect and disorder cells.

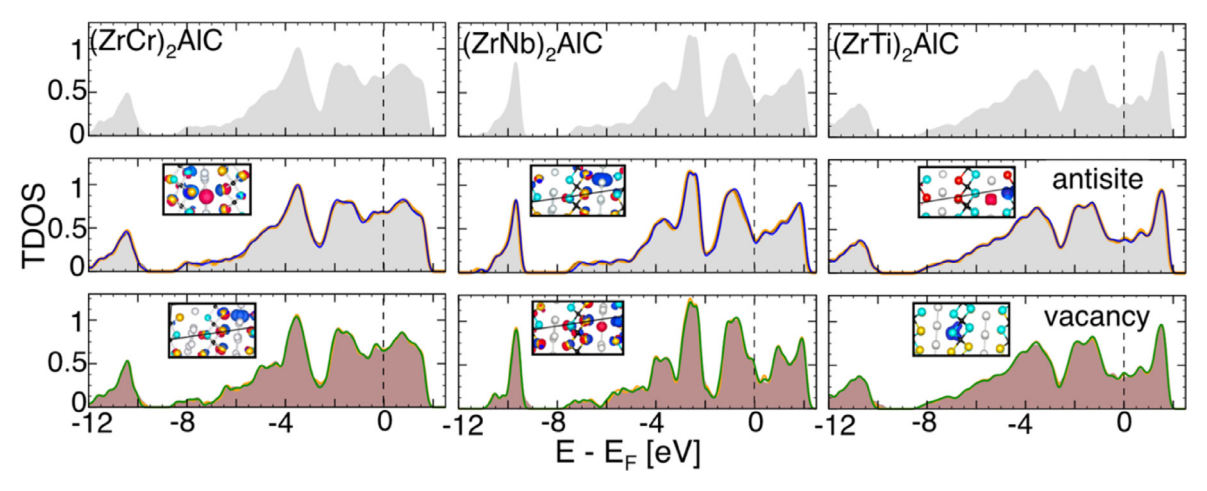


Fig. 5. The total DOS of the pure (top), antisite (middle) disorder and monovacancy (bottom) defects in (M-M')2AlC (M=Zr; M'=Cr,Nb,Ti).

that interchanging the M- and A-cation position with X-anions costs more energy than anion-anion interchange.

The charge density difference between disorder $(Zr-M=Cr)_2AlC$ with and without antisite defects in Fig. 4e shows large charge transfer due to in-plane Zr-d/Cr-d interactions. The Zr-Cr/Zr-Zr/Cr-Cr bonds in $(ZrCr)_2AlC$ are populated with in-plane Zr-Cr/Zr-Zr/Cr-Cr bonds, respectively, whereas the in-plane Zr-Cr/Zr-Zr/Cr-Cr bonds are emptied in favor of the Zr-Cr/Zr-Zr/Cr-Cr bonds are emptied in favor of the Zr-Cr/Zr-Zr/Cr-Cr basal bonds. This helps us understand the reason behind the increased stability of the Zr/Cr-C layers in the $(ZrCr)_2AlC$ system. To exemplify, we plot Ti_2AlC and Ta_2AlC band structure in Fig. S7 that shows metallic behavior in the basal plane with multiple bands crossing at the Fermi-level (E_{Fermi}) while no bands cross the E_{Fermi} in c-direction along $(\Gamma-A)$.

3.4. Electronic properties

In Fig. 5, we show the total density of state of disordered (Zr-M)₂AlC MAX phases for M=Cr, Nb and Ti. The transition elements Zr, Cr, Nb and Ti have partially filled bonding d-states (also see Fig. S8), which means that the electrons at E_{Fermi} are mainly from

M elements and form conducting bands. If we look at the partial DOS of the Zr₂AlC and Cr₂AlC in Fig. S8, the Zr-d and Cr-d states in (-5.5 eV to -2.5 eV) and (-8.5 eV to -5 eV) energy range, respectively, overlap significantly with the C-p states. Alloying Cr with Zr in Zr₂AlC adds more electrons that increases the DOS near the E_{Fermi} (Fig. 5), i.e., Cr addition increases the localized d-states. This also means that Zr-d/Cr-d & C-p in the alloy form strong covalent bonds, while, the Al-p with Zr-d and Cr-d states in the energy range -3 eV to 0 eV and -5 eV to -2 eV show a weaker hybridization, respectively. This suggests metallic bonding between Al-p and M-d states.

We note on comparing TDOS of $(Zr-M)_2AlC$ in Fig. 5 with antisite (middle) and vacancy (bottom) defects that the peaks in density of states near the E_{Fermi} for vacancy cases changes greatly due to increased hybridization. However, this depends on type of vacancy, i.e., V_M , V_A , or V_X , which alters the electronic density and the strength of hybridization near E_{Fermi} as the V_M and V_C reduces the number of M-C bonds. On the contrary, for VA, the neighboring atoms readjusts itself to maintain the energy stability by charge transfer. Comparing total DOS for the systems with (bottom panel) and without (top panel) vacancies, we could

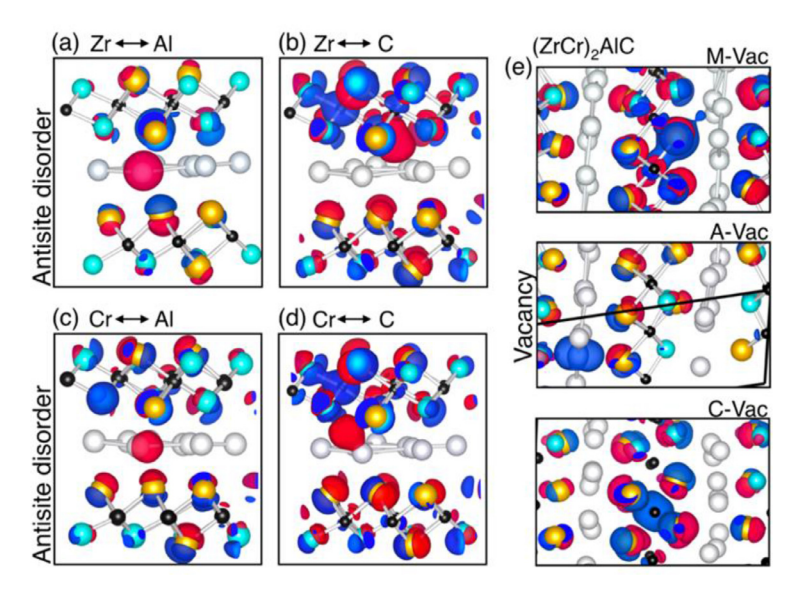


Fig. 6. Charge difference of M-site disorder (ZrCr)₂AlC MAX phase with (a–d) antisite disorder and (e) V_M, V_A and V_x vacancies. Clearly, antisite and vacancy defect changes the local chemical activity by stronger charge transfer.

clearly see the hybridization peak in the same energy range near the E_{Fermi} for vacancy cases. We attribute this to the reduced numbers of M-A bonds. Notably, no such changes are observed for the case of antisite defects as system's electronic density (only atomic positions are interchanged) remains conserved

To further investigate this, we plot the charge density difference between vacancy and no-vacancy cases in the inset Fig. 5. The DOS above the E_{Fermi} is the result of weaker Zr-d/Cr-d and Al-p bonding with a little contribution form the C-p states (also see supplementary material). On the other hand, the top of the valance band is formed by Zr-d/Cr-d, C-p and Al-p hybridized states. For the ordered MAX phase, in Fig. S8, the states at the E_{Fermi} are mainly from the Zr-d/Cr-d, C-p and Al-p with a small contribution of C-p.

3.5. Charge density difference of antisite and vacancy defects with disorder $(ZrCr)_2AlC$

The MAX phases form M-X, M-A, and A-A bonds, where M-X is the covalent and A-A is the metallic bond, respectively. This is the reason why M-X bonds are stronger than A-A bonds. If we compare two ordered MAX phases, e.g., Zr_2AIC and Cr_2AIC , the Zr_2AIC compounds are weaker than the Cr-based compounds due to significant difference in χ between Zr and Zr (Zr = 1.33, Zr = 1.66). Large Zr of Zr of Zr attracts more charges and makes the bonds in Zr of Zr stronger. This also suggests that Zr all will have more agility towards re-organizing defects compared to Zr of Zr due to vacancy formation as shown in Zr of Zr by charge density difference between pure and defect (Zr Zr) alc. For example, the cationic defects lead to much stronger bonding between Zr or Zr viz. Zr Zr or Zr and Zr or Zr

Our calculations show that both alloying and defects (antisite/vacancy) can be used as effective tools to tailor the properties of MAX phases. For example, alloying Zr₂AlC with an smaller size atom Cr (R=0.76 Å) at Zr-site (R=0.86 Å) increases the C-Cr interaction compared C-Zr by redistributing the electronic-density in and around the A-layer. We believe that the electronic rearrangement plays an important role in the increased stability of (ZrCr)₂AlC. Electronegativity is another factor important to understand the chemical bonding. Following the Pauling electronegativity scale (χ_{Cr} =1.66, χ_{Zr} =1.33, χ_{Al} = 1.61 and χ_{C} = 2.55), we find a significant charge transfer from Zr/Cr to

C in (ZrCr)2AlC as shown in Fig. 6, where the directional Zr/Cr-C bonding leads to covalent character. The driving force behind the displacement of the bonding charges from Zr/Cr to C is due to the greater ability of C to attract electrons as a result of the difference between atomic electronegativities ($\Delta \chi = \chi_M - \chi_C$).

3.6. Vacancy migrations energies

Vacancies are the most common defects at equilibrium and they greatly control the kinetics of diffusion-mediated processes. For high-temperature applications, vacancy diffusion is an important aspect to explore, particularly because the exchange between vacancies and atoms in the lattice is often times the limiting step when considering possible chemistry-driven transformations, including the selective oxidation of Al in Al-containing MAX phases, for example. To date, very little progress has been made towards increasing the understanding of vacancy diffusion mechanism in disordered MAX phases from a theoretical framework—we note that a companion paper from the present group explicitly looks at migration energies of vacancies for a large number of pure 211 MAX phase systems [49].

We study V_M , V_A , and V_X migration in disordered MAX phases as shown by schematic in Fig. 7. We use cNEB to generate a succession of configurations (images) along the initial band connecting the initial-to-final state and calculate vacancy formation energies. cNEB relaxes each state on the band and provides information for deforming that band towards a lower energy embedding in the potential energy landscape. The band location in the energy landscape after sufficient number of iterations corresponds to the minimum path connecting the reactants and products.

In Fig. 8(a-c), we plot the V_M , V_{Al} , and V_C migration energies for five ordered MAX phase compounds: M_2AlC , M=Ti, Ta, Cr, Nb, Zr. The Zr_2AlC shows lowest energy barrier for V_M , V_{Al} , and V_C compared to all other cases, where V_{Al} has the smallest barrier height. The overall order of vacancy migration energy for ordered MAX phases is $V_M > V_C > V_{Al}$ with the Zr_2AlC as the only exception, where V_M has lower migration energy than V_C . Comparing E_{form}^{Vac} in Fig. 1b with barrier energy in Fig. 8a-c of ordered MAX phases, we can make the inference that stable V_{Al} is easier to move within the basal plane than other vacancies. In spite of competing migration energies of V_M and V_C in Zr_2AlC , E_{form}^{Vac} is in sharp contrast in term of energy stability in Fig. 1b. Higher

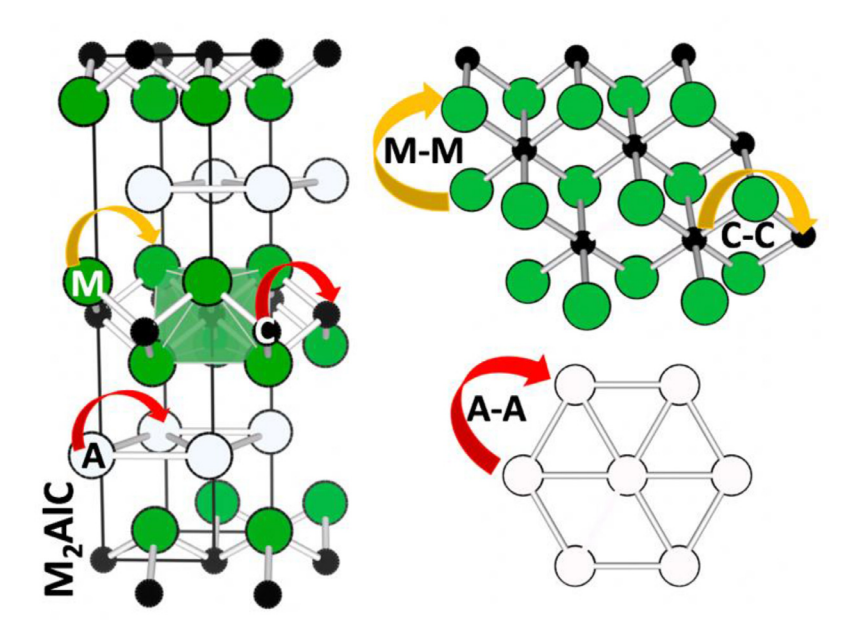
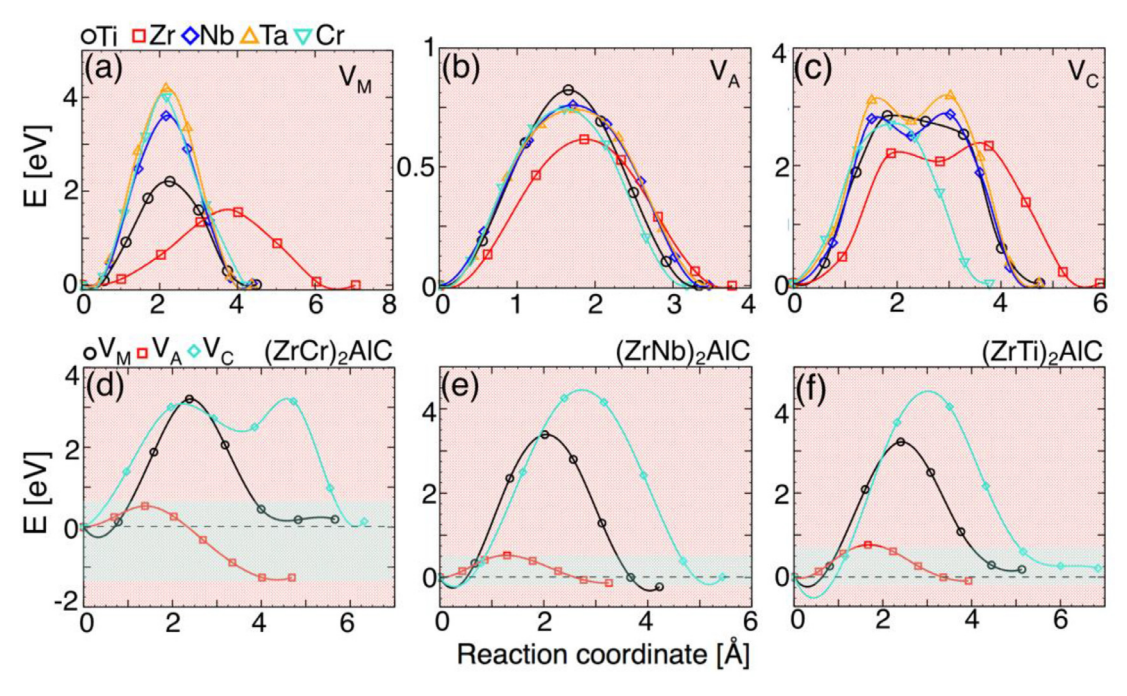


Fig. 7. Schematic of V_M, V_A and V_C vacancy migration in order and disorder MAX phase alloy.



 E_{form}^{Vac} for Zr_2AlC suggest that vacancies are hard to create, while (relatively) low diffusion barriers suggest facile vacancy migration.

The vacancy migration barrier for disordered $(ZrM)_2AlC$ in Fig. 8(d-f) follows the trend of E_{form}^{Vac} in Fig. 3, where A-site migration is easier in $(ZrNb)_2AlC$ compared to $(ZrCr)_2AlC$ and $(ZrTi)_2AlC$, i.e., E_{mig} [$(ZrCr)_2AlC$] > E_{mig} [$(ZrTi)_2AlC$] > E_{mig} [$(ZrNb)_2AlC$]. The barrier hights in Fig. 8(d-f) for the disordered MAX phases shows great dependence on the local environment. This is further established by zero end-point energies in ordered MAX phases, whereas the non-zero end-point energies in disorder MAX phases are configuration dependent. Creating two vacancies at symmetrically related Wycoff-positions changes the neighbor distributions, which

affects the total energy of the vacancy supercell. The vacancy formation energies and vacancy concentration can directly be connected. If we compare vacancy formation energies from Fig. 2, e.g., the lower and comparable formation energies of $(ZrNb)_2AlC$ and $(ZrTi)_2AlC$ will allow larger vacancy concentration compared to $(ZrCr)_2AlC$. Similarly, for $(ZrM)_2(AA')C$, the V_A vacancy migration in $(ZrM)_2AlC$ within the basal plane is easier and proceeds with an energy barrier of 0.5 to 1.0 eV. This is much lower than the V_M or V_C vacancy migration barrier. However, the high-migration energy makes V_M diffusion unfavorable compared to V_A and V_X . Therefore, the significant population of the vacancies created in M-layers may remain intact even after a significantly long time.

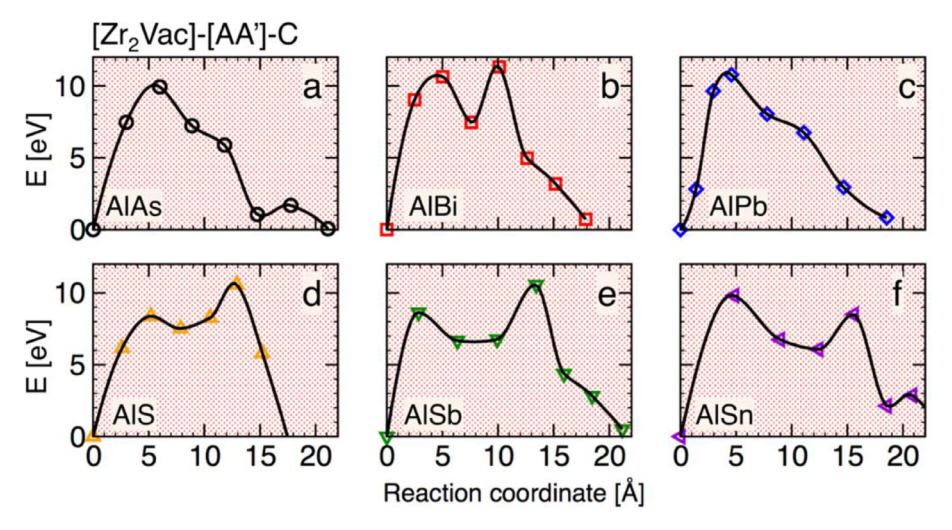


Fig. 9. (a-f) The M-site (V_M) vacancy migration barrier for A-site disorder for $Zr_2(A-A')C$, A=Al, A'=As, Bi, Pb, S, Sb, Sn. The energy threshold (activation energy) must be overcome for vacancy migration. With A-site disorder, vacancy migration at Zr-site becomes harder.

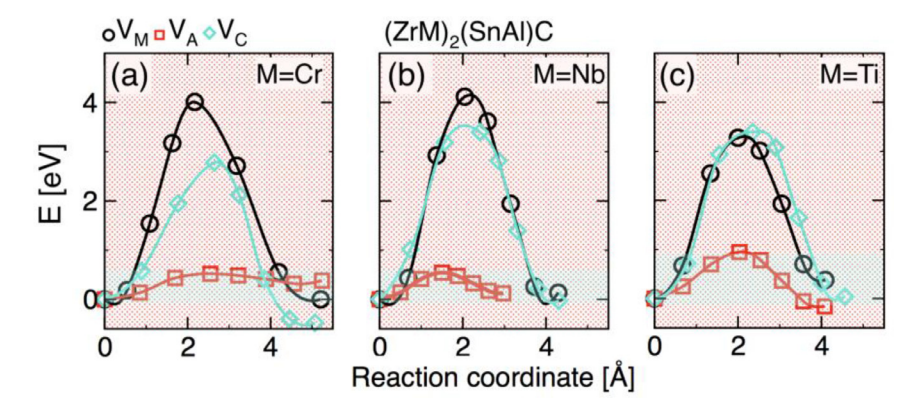


Fig. 10. The V_M, V_A and V_C vacancy migration energies of MAX alloys with M- and A-site disorder using cNEB method: (M-M')₂(A-A')C, M=Zr, M'=Cr,Nb,Ti, A=Sn and A'=Al.

In Fig. 9 and Fig. 10, we present barrier energy for A-site disorder $[Zr_2(A-A')C, A=Al, A'=As, Bi, Pb, S, Sb, Sn]$ and two (M and A)site disorder ((Zr-M)₂(A-A')C, where M=Cr,Nb,Ti and A-A'=SnAl), respectively. The vacancy migration energies in Fig. 9 shows very high barrier height ranging from 9-12 eV for A-site disorder with V_M. The high barrier makes vacancy diffusion almost impossible, however, once the vacancies are created, a significant population of the vacancies will be intact for a considerable time under the irradiation process. On the other hand, for two-site disorder with V_M , V_A and V_C vacancies in Fig. 10 (also see Fig. S6), the diffusion barrier show competing energies for V_M and V_C for M=Nb and Ti. The A-site vacancies for M=Cr show almost barrierless diffusion. If compared to single M-site disorder migration energies as presented in Fig. 8d-f, adding more disorder, i.e., to both to Mand A-site, further improves the vacancy diffusion by reducing the barrier height. The V_{M} and V_{X} site vacancies show competing E_{form}^{Vac} in Fig. 3b, but vacancy migration becomes easier for V_A with small barrier size of 0.40 eV due to increased chemical disorder.

4. Conclusions

MAX phases are very exciting new class of materials because of their high-temperature applications and the vacancies are most common defects at high operating conditions. Therefore, we set out the main objective of this work to find out: (1) How the role of vacancies changes in going from order to disorder MAX phases; and (2) Can we use alloying in combination with vacancies as an effective tool to tailor MAX phase properties? We perform

first-principles DFT calculations to explore the alloying effect on the structural-stability, energy-stability, electronic-structure, and vacancy diffusion of MAX phases. Both as a test-bed and useful application in nuclear engineering, Zr₂AlC was an interesting example to be explored for the effect of alloying and defect formation because the lower formation energy of ordered Zr₂AlC suggests the possibility of higher vacancy concentration which may in turn be beneficial for the production of protective passive oxide layers.

We considered single-site (M-/A-) and two-site (M-A) disorder and explored the vacancy and antisite defect stability. We found that disordering has a significant effect on energy-stability, electronic-structure and vacancy migration behavior of (Zr-M')2(A-A')X (M = Cr, Nb, Ti, AA' = Al, SnAl, X = C), whereas in some cases antisite defects are much easier to form compared to point vacancies. For example, Al preferentially goes to Cr compared to Zr in Cr-doped Zr₂AlC, i.e., (ZrCr)₂AlC. Other focus of this work was to understand the effect of chemical alloying and defects on vacancy diffusion profile of MAX phases. While the diffusion barrier in strongly bonded metal alloys is usually large, our DFT+cNEB calculations show that alloying helps in lowering down both vacancy formation energy and diffusion-barrier compared to ordered MAX phases. The reduced barrier height for Al-diffusion as found in our study through alloying is an important finding because Al is known to promote the formation of protective oxide layer (i.e., Al₂O₃ in aluminum-based MAX phases) at high-operating temperatures. Therefore, the reduced vacancy formation energy and barrier height will help the formation of protective oxide layer in Al-based MAX phases. Based on our study, we believe that the chemical alloying route will surely help the MAX phase community to understand the defect formation and migration mechanism as well as provide ways to manipulate the electronic and mechanical behavior of MAX phases.

Declaration of Competing Interest

None

Acknowledgments

Valuable discussion with Dr. M. Radovic is acknowledged. The financial support was provided from National Science Foundation through grants no. (DMREF) CMMI-1729350. First-principles calculations were carried out at the Supercomputing Facility at Texas A&M University. DS acknowledges the support of NSF through grant no. NSF-DGE-1545403.

Supplementary materials

Supplementary material associated with this article can be found, in the online version, at doi:10.1016/j.actamat.2019.11.033.

References

- [1] M.W. Barsoum, MAX Phases: Properties of Machinable Carbides and Nitrides, Wiley VCH, 2013.
- [2] M. Radovic, M.W. Barsoum, MAX phases: bridging the gap between metals and ceramics, Am. Ceram. Soc. Bull. 92 (2013) 20-27.
- [3] M.W. Barsoum, M. Radovic, Elastic and mechanical properties of the max phases, Annul. Rev. Mater. Res. 41 (2011) 195-227.
- [4] J. Wang, Y. Zhou, Recent progresses in theoretical prediction, preparation and characterization of layered ternary transition metal carbides, Annul. Rev. Mater. Res 39 (10) (2009) (1-29).
- [5] Z. Lin, M. Li, Y. Zhou, TEM investigation on layered ternary ceramics, J. Mater. Sci. Technol. 23 (2007) 145.
- [6] E.N. Hoffman, D.W. Vinson, R.L. Sindelar, D.J. Tallman, G. Kohse, M.W Barsoum, MAX phase carbides and nitrides: properties for future nuclear power plant in-core applications and neutron transmutation analysis, Nuclear Eng. Des. 244 $(2012)\ 17-24.$
- [7] M. Naguib, V.N. Mochalin, M.W. Barsoum, Gogotsi, Y. MXenes, A new family of two-dimensional materials, Adv. Mater. 26 (2014) 992-1005.
- M. Naguib, M. Kurtoglu, V. Presser, J. Lu, J. Niu, M. Heon, L. Hultman, Y. Gogotsi, M.W. Barsoum, Two- Dimensional Nanocrystals produced by exfoliation of Ti₃AlC₂, Adv. Mater. 23 (2011) 4248-4253.
- [9] T. Ito, S. Okazaki, Pushing the limits of lithography, Nature 406 (2000) 1027.
- [10] K. Sickafus, et al., Radiation tolerance of complex oxides, Science 289 (2000) 748-751
- [11] K.E. Sickafus, et al., Radiation-induced amorphization resistance and radiation
- tolerance in structurally related oxides, Nat. Mater. 6 (2007) 217–223. [12] C. Wang, T. Yang, C.L. Tracy, C. Lu, H. Zhang, Y.-J. Hu, L. Wang, L. Qi, L. Gu, Q. Huang, J. Zhang, J. Wang, J. Xue, R.C. Ewing, Y. Wang, Disorder in $m_{n+1}ax_n$ phases at the atomic scale, Nat. Commun. 10 (2019) 622.
- [13] P. Eklund, M. Beckers, U. Jansson, H. Högberg, L. Hultman, The $m_{n+1} a x_n$ phases: materials science and thin film processing, Thin Solid Films 518 (2010) 1851.
- [14] K. Nordlund, J. Keinonen, M. Ghaly, R.S. Averback, Coherent displacement of atoms during ion irradiation, Nature 398 (1999) 49-51.
- [15] Y. Zhang, et al., Ionization-induced annealing of pre-existing defects in silicon carbide, Nat. Commun. 6 (2015) 8049.
- [16] Y. Zhang, et al., Influence of chemical disorder on energy dissipation and defect evolution in concentrated solid solution alloys, Nat. Commun. 6 (2015) 8736.
- [17] G.S. Was, R.S. Averback, in: R.J.M. Konings (Ed.), Comprehensive Nuclear Materials, Vol. 1, Elsevier Ltd, 2012, pp. 293-332.
- [18] W. Jager, M. Wilkens, Phys. formation of vacancy-type dislocation loops in tungsten bombarded by 60keV au ions, Status Solidi 32 (1975) 89.

- [19] T. Liao, J.Y. Wang, Y.C. Zhou, First-principles investigation of intrinsic defects and (N, O) impurity atom stimulated al vacancy in Ti2AlC, Appl. Phys. Lett. 93 (2008) 261911.
- [20] S.I. Zhao, I.M. Xue, Y.G. Wang, O. Huang, Ab initio study of irradiation tolerance for different mn+1axn phases: ti₃SiC₂ and Ti₃AlC₂, J. Appl. Phys. 115 (2014)
- [21] L.F. Marion, I. Monnet, Saturation of irradiation damage in (Ti,Zr)₃(Si,Al)C₂ compounds, J. Nucl. Mater. 433 (2013) 534-537.
- [22] Y.G. Xu, X.D. Ou, X.M. Rong, Vacancy trapping behaviors of hydrogen in
- Ti3SiC2: a first-principles study, Mater Lett 116 (2014) 322–327.
 [23] X.D. Ou, Y.X. Wang, I.Q. Shi, W. Ding, M. Wang, Y.S. Zhu, Effect of hydrogen– doping on bonding properties of Ti₃SiC₂, Physica B 406 (2011) 4460-4465
- [24] J.R. Xiao, C.X. Wang, T.F. Yang, S.Y. Kong, J.M. Xue, Y.G. Wang, Theoretical investigation on helium incorporation in Ti₃AlC₂, Nucl. Instr. Meth. Phys. Res. B 304 (2013) 27–31
- [25] S.C. Middleburgh, G.R. Lumpkin, D Riley, Accommodation, accumulation, and migration of defects in Ti3SiC2 and Ti3AlC2 max phases, J. Am. Ceram. Soc. 96 (2013) 3196-3201.
- [26] K. Nordlund, J. Keinonen, M. Ghaly, R. Averback, Coherent displacement of atoms during ion irradiation, Nature 398 (1999) 49.
- [27] B.D Wirth, How does radiation damage materials, Science 318 (2007) 923-924.
- [28] A.A. Balandin, Thermal properties of graphene and nanostructured carbon materials, Nat. Mater. 10 (2011) 569–581.
- [29] R. Noriega, et al., A general relationship between disorder, aggregation and
- charge transport in conjugated polymers, Nat. Mater. 12 (2013) 1038.

 [30] C. Meneghini, et al., Nature of "disorder" in the ordered double perovskite Sr₂FeMoO₆, Phys. Rev. Lett. 103 (2009) 046403.
- [31] D.J. Tallman, B. Anasori, M.W. Barsoum, A critical review of the oxidation of Ti₂AlC, Ti₃AlC₂ and Cr₂AlC in air, Mater. Res. Lett. 1 (2013) 115-125.
- [32] A. Zunger, S.H. Wei, L.G. Ferreira, J.E Bernard, Special quasirandom structures, Phys. Rev. Lett. 65 (1990) 353-356.
- [33] A. van de Walle, P. Tiwary, M.M. de Jong, D.L. Olmsted, M. Asta, A. Dick, D. Shin, Y. Wang, L.-Q. Chen, Z.-K. Liu, Efficient stochastic generation of special quasirandom structures, Calphad 42 (2013) 13-18.
- [34] G. Makov, M.C. Payne, Periodic boundary-conditions in ab-initio calculations, Phys. Rev. B 51 (1995) 4014-4022.
- [35] S. Lany, A. Zunger, Assessment of correction methods for the band-gap problem and for finite-size effects in supercell defect calculations: case studies for zno and gaas, Phys. Rev. B 78 (2008) 235104.
- [36] G. Kresse, J. Hafner, Ab initio molecular dynamics for liquid metals, Phys. Rev. B 47 (1993) 558-561.
- [37] G. Kresse, D. Joubert, From ultrasoft pseudopotentials to the projector augmented-wave method, Phys. Rev. B 59 (1999) 1758-1775.
- [38] H.J. Monkhorst, J.D. Pack, Special points for brillouin-zone integrations, Phys. Rev. B 13 (1976) 5188-5192.
- [39] J.P. Perdew, K. Burke, M Ernzerhof, Generalized gradient approximation made simple, Phys. Rev. Lett. 77 (1996) 3865-3868.
- [40] G. Henkelman, B.P. Uberuaga, H. Johnsson, A climbing image nudged elastic band method for finding saddle points and minimum energy paths, J. Chem. Phys 113 (2000) 9901-9904.
- [41] S.C. Middleburgh, R.W. Grimes, Defects and transport processes in beryllium, Acta Mater 59 (2011) 7095-7103.
- [42] H. Tahini, A. Chroneos, R.W. Grimes, Diffusion of e centers in germanium predicted using gga+u approach, Appl. Phys. 99 (2011) 072112 (1-3).
- [43] L. Kun, Q. Yuan, D. Ji-Zheng, First-principles investigation of the vacancy effect on the electronic properties in M_2AlC (M = v and nb), AIP Adv 4 (2014)
- [44] J.Y. Wang, Y.C. Zhou, T. Liao, J. Zhang, Z.J. Lin, A first-principles investigation of the phase stability of Ti₂AlC with Al vacancies, Scripta Mater 58 (2008)
- [45] T. Liao, J.Y. Wang, Y.C. Zhou, A first-principles investigation of the phase stability of Ti₂AlC with Al vacancies, Scripta Mater 59 (2008) 854-857.
- [46] B. Meyer, M. Fähnle, Ab initio calculation of the formation energy and the formation volume of monovacancies in Mo, Phys. Rev. B 56 (1997) 13595-13598.
- [47] H. Yao, L. Ouyang, W.Y. Ching, Ab initio calculation of the elastic constants of ceramic crystals, J. Am. Ceram. Soc. 90 (2007) 3194-3204.
- [48] A. Talapatra, T. Duong, W. Son, H.Radovic Gao, R. Arroyave, High-throughput combinatorial study of the effect of M site alloying on the solid solution behavior of M2AIC max phases, Phys. Rev. B 94 (2016) 104106 (1-15).
- [49] A. Talapatra, M. Radovic, R. Arroyave, High-throughput investigation of vacancy formation and migration energies in 211 max phase systems, unpublished,